Coagulation of nanoparticles in a plasma

Lavanya Ravi and Steven L. Girshick
Department of Mechanical Engineering, University of Minnesota, Minneapolis, Minnesota 55455, USA
(Received 18 August 2008; revised manuscript received 2 February 2009; published 27 February 2009)

Coagulation of nanoparticles in a low-pressure radio frequency plasma was studied by means of a detailed numerical model for the spatiotemporal evolution of the nanoparticle-plasma system. Simulation results indicate that the occurrence of coagulation to any significant degree in such systems requires the existence of two effects: first, gas-phase nucleation is not limited to a brief burst, but rather continues in regions that are sufficiently free of nanoparticles; and second, coagulation coefficients for collisions between neutral and negatively charged nanoparticles are enhanced by the image potential induced in the neutral particle. Accounting for these effects, coagulation is predicted to be dominated by coagulation between very small (~1 or 2 nm in diameter) neutral particles and larger negatively charged particles that are trapped in the plasma. Coagulation ceases when the spreading of the nanoparticle cloud across the plasma quenches gas-phase nucleation.

DOI: 10.1103/PhysRevE.79.026408 PACS number(s): 52.27.Lw, 52.65.−y, 81.20.Rg

I. INTRODUCTION

Coagulation in nanodusty plasmas—plasmas containing nanoparticles—is of interest for several reasons. First, coagulation in nanodusty plasmas is believed to be the primary means by which particles grow to several tens of nanometers in diameter following their initial formation via gas-phase nucleation [1–7]. Such particles often represent an unacceptable source of contamination in semiconductor processing. Second, particle morphology can be strongly affected by coagulation, and this has implications for the deliberate synthesis of nanocrystals for various applications. Finally, coagulation in nanodusty plasmas is of fundamental interest, but is poorly understood.

The most studied nanodusty plasma has been the capacitatively coupled parallel-plate radio frequency (rf) plasma, consisting of silane diluted in argon or helium, at total pressures in the range ~10–100 Pa. In the early 1990s experimental observations by Boufendi, Bouchoule, and coworkers led them to conclude that the temporal evolution of nanoparticles in such a system could be described by a three-step process: a brief nucleation burst, lasting several ms and producing particles ~2 nm in diameter; rapid growth by coagulation, producing particles up to a few tens of nm in diameter; and then slower growth by vapor deposition on particle surfaces [1–3].

The inference in these studies that the rapid growth phase following nucleation is dominated by coagulation was based primarily on two observations. First, as the average particle size increased, the measured particle concentration dropped while the total particle mass concentration stayed approximately constant. Second, images of sampled particles obtained by transmission electron microscopy showed particles that appeared to be aggregates of smaller crystallites, typically ~2 nm in size [1,2].

Nevertheless, there are grounds for questioning whether coagulation to any significant extent is likely or even possible in such systems. As particles grow in these types of plasmas they become increasingly negatively charged. If all of the particles were negatively charged then coagulation would be almost completely suppressed by Coulomb repulsion. However, in the earliest times following the onset of nucleation, when particles are only 1 or 2 nm in diameter, measured particle concentrations [1] are in the order of 10^9–10^{10} cm^{-3}, and many of these particles may be neutral. That is because such small particles can hold at most one or two charges [8], so that stochastic charge fluctuations due to discrete charging events ensure that at any time many of the particles are neutral or even positively charged. Moreover, the particle concentration produced in the initial nucleation burst may exceed the plasma density that existed prior to the appearance of particles. In that case there would not be enough electrons available to immediately charge all of the particles negatively.

As for Brownian coagulation between neutral particles, the characteristic time for coagulation under these conditions is much longer than the characteristic time for loss of particles to bounding surfaces by diffusion. For neutral aerosol particles that lie in the free molecule regime (an excellent assumption for the conditions of interest), assuming spherical particles and unity sticking coefficients, and neglecting the effect of van der Waals forces, the coagulation coefficient $\beta(v_i,v_j)$ (m^3 s^{-1}) for particles of volumes v_i and v_j can be written [9]

$$\beta(v_i,v_j)=\left(\frac{3}{4\pi}\right)^{1/6}\left[\frac{6kT}{\rho_p}\left(\frac{1}{v_i}+\frac{1}{v_j}\right)\right]^{1/2}(v_i^{1/3}+v_j^{1/3})^2, \quad (1)$$

where k is the Boltzmann constant, T is absolute temperature, and ρ_p is the mass density of the material of which the particles are composed. The characteristic time for coagulation of an assumed monodisperse aerosol can be estimated as

$$\tau_{coag}=\frac{2}{\beta N_p}, \quad (2)$$

where τ_{coag} is the time required for coagulation to reduce the particle concentration N_p by one-half. For 2-nm particles at 300 K having the same mass density as bulk silicon (2.33 g/cm^3), Eq. (1) gives $\beta \approx 5.8\times10^{-10}$ cm^3/s. For particle concentrations of 10^9–10^{10} cm^{-3}, one finds $\tau_{coag} \approx 0.34$–3.4 s.

One can also define a characteristic time τ_{diff} for particles to diffuse a distance Λ as

$$\tau_{diff} = \frac{\Lambda^2}{2D}, \tag{3}$$

where D is the particle diffusion coefficient in the ambient gas. For 2-nm-diameter spherical particles in argon at 100 mTorr (13.3 Pa) and 300 K, $D \approx 86$ cm^2/s. Taking Λ as half the plate separation, for a plate separation of 3 cm, one finds $\tau_{diff} \approx 0.013$ s, much less than τ_{coag}. Thus, under such conditions, neutral particles would be lost by diffusion before they had time to coagulate with each other.

Higher particle concentrations and/or higher pressures could make τ_{coag} and τ_{diff} more comparable to each other. Even then, however, one confronts the fact that as particles grow they become, on average, more negatively charged. Whereas neutral and positively charged particles are rapidly lost by diffusion, negatively charged particles are trapped in the plasma by the electric field, allowing them to continue growing by vapor deposition. Finally, if all the neutral particles produced at the earliest times were lost by diffusion, while only multiply charged negative particles remained, how could coagulation be sustained up to the particle diameters claimed, e.g., ~50 nm in diameter [1,2,4,5,10], well beyond the size where all particles are expected to be negatively charged?

Recently Warthesen and Girshick developed a detailed model for the spatiotemporal evolution of a nanodusty plasma [11], with the plasma behavior and the aerosol behavior treated self-consistently. Simulations were run for the same conditions as in the experimental work of Boufendi, Bouchoule, and co-workers [1–3]. Particle nucleation was assumed to occur only in a rapid burst, lasting 10 ms. The results of these simulations indicated that coagulation was almost nonexistent. Consistent with the discussion above, the neutral particles produced in the initial nucleation burst were either lost to the walls by diffusion, before they experienced significant coagulation, or became negatively charged and trapped. Whereas a singly charged particle could be rapidly neutralized by ion attachment, once particles were more than a few nm in diameter they were mostly multiply charged, and therefore unlikely to be neutralized. Thus the system rapidly evolved to one in which all particles were charged negatively, with coagulation suppressed. Turning coagulation on or off in the simulations made no discernible difference in the results.

In this paper we address the question, how can coagulation occur in a nanodusty plasma, given the arguments against its existence presented above? We first review work that suggests a possible way out of this dilemma, namely, that two distinct aerosol populations coexist in the plasma, one consisting of large, negatively charged particles, the other of much smaller particles, many of which are neutral or positively charged. We then report numerical simulations that use the same numerical model as Warthesen and Girshick [11], but with two important changes. First, instead of limiting nucleation to a brief burst, it is allowed to continue in regions that are sufficiently free of particles. Second, we account for the effect on coagulation of the image potential (dipole) induced in neutral particles in proximity to charged particles. With these two changes, we find that coagulation indeed becomes an important growth mechanism. But it is predicted to be a very specific kind of coagulation—scavenging of small neutral particles by larger charged particles—and it is highly localized, because of the quite different spatial profiles of charged and neutral particles. These results support the hypothesis that coagulation in a nanodusty plasma occurs primarily between two distinct particle populations, and put this hypothesis in the context of the spatiotemporal evolution of the nanoparticle-plasma system. Also these results indicate that coagulation in low-pressure nanodusty plasmas would be negligible were it not for both the continued occurrence of fresh nucleation and the enhancement in the rates of coagulation between neutral and charged nanoparticles caused by image potentials.

II. COAGULATION BETWEEN POPULATIONS OF PARTICLES HAVING DIFFERENT SIZES

Several researchers have suggested that coagulation in dusty plasmas could occur between particle populations of distinctly different sizes: one large, the other small. This hypothesis has several advantages. First, from Eq. (1), Brownian coagulation coefficients are much larger for particles of widely disparate sizes than for particles of the same size. This is because the larger collision cross section more than offsets the slower thermal speed of the larger particles. Second, very small particles in such systems may be neutral or even positively charged, allowing them to coagulate with larger, negatively charged particles that are trapped in the plasma. Third, this hypothesis would be consistent with the experimental observation that larger particles are composed of ~2-nm crystallites [1,2]. Finally, coagulation rates between large, highly charged particles and small neutral particles can be strongly enhanced by the image potential induced in the neutral particle.

Horanyi and Goertz suggested that coagulation in a dusty plasma could occur between small and large particles of opposite charge [12], although their work did not consider particles in the nanoscale regime and was more concerned with astrophysical plasmas where secondary electron emission could be an important mechanism producing positively charged particles. Shiratani, Watanabe, *et al.*, in work that studied particle formation in silane plasmas [5,10], used scanning electron microscope images of sampled particles to deduce the existence of two distinct particle size classes. Observing that measured particle growth rates were much higher than could be explained by Brownian coagulation, they too proposed that coagulation occurred mainly between particles of opposite charge, with the smaller particles charged positively by stochastic charge fluctuations. Lemons *et al.* proposed a simple analytical model for coagulation between large "predator" particles and smaller "protoparticles" that were injected into a plasma at a constant rate, with the predator particles charged negatively while the protoparticles were mostly neutral [13]. They assumed that the protoparticles were too small to hold a charge, which they determined corresponded to a diameter below 2.4 nm, or that

they could be somewhat larger if one accounted for charge fluctuations. Their model, while containing only minimal physical content, succeeded in reproducing the particle growth rates reported by Boufendi and Bouchoule [14] and Shiratani *et al.* [4]. Kim and Kim developed a more detailed numerical model for coagulation between large and small particles in a plasma, with each size class having an assumed Gaussian charge distribution [15–17]. They utilized a sectional model for the particle size distribution function, with size-dependent coagulation coefficients, and included the effect of Coulomb forces for coagulation between oppositely charged particles. The latter effect was predicted by their model to dominate coagulation. De Bleecker *et al.* also used a sectional approach to model coagulation in a plasma [18], although they neglected the effect of particle charge on coagulation rates.

None of the above studies considered the possible effect on coagulation of image potentials induced in colliding particles by the charge on the collision partner. To our knowledge the only plasma-related study to have considered this effect is the work of Lapenta, who developed a simple analytical model based on conditions of dust grains in stellar systems, with a high relative velocity between the dust grains and the stellar wind [19]. He concluded that dipole moments could lead to the production of linear chainlike aggregates.

A theoretical analysis of the enhancement in coagulation coefficients in an aerosol due to image potentials induced in a neutral particle by a charged particle was presented by Huang, Okuyama, and Seinfeld [20]. The enhancement factor is a complicated function of the diameters of the colliding particles, the mean free path for molecular collisions in the gas, the magnitude of the charge on the charged particle, and the dielectric constant of the material of which the particles are composed.

The magnitude of the effect for conditions pertinent to nanodusty plasmas is seen in Fig. 1, which shows coagulation coefficients between a 1-nm-diameter particle and a second particle of any diameter up to 100 nm, for three cases: (i) both particles are neutral, from Eq. (1); (ii) the 1-nm particle is singly positively charged while the second particle is negatively charged; and (iii) the 1-nm particle is neutral while the second particle is charged. In all cases we assume spherical particles with the properties of bulk silicon, and the gas is assumed to consist of argon at a pressure of 13.3 Pa and a temperature of 300 K. In cases (ii) and (iii) the negatively charged particle is assumed to have a charge equal to the average charge on negatively charged particles of the same size, based on the full simulation results presented below.

For the case of oppositely charged particles, the Coulomb attraction causes the coagulation coefficient in Eq. (1) to be multiplied by a factor γ given by

$$\gamma = 1 - \frac{Z_1 Z_2}{4\pi\varepsilon_0 kT(r_1 + r_2)}, \tag{4}$$

where Z_i represents the charge on each of the two particles (Z_1=unit charge), r_i is the radius of each particle (r_1 =0.5 nm), and ε_0 is the permittivity of free space [9]. For the case of coagulation between a 1-nm neutral particle and a

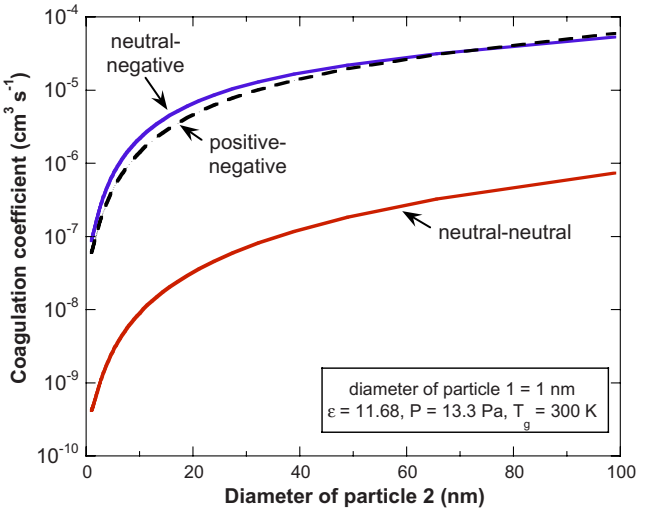

FIG. 1. (Color online) Coagulation coefficients between particles that are 1 nm in diameter (particle 1) and particles of any diameter (particle 2). The three cases shown are for neutral coagulation [Eq. (1)], coagulation of oppositely charged particles, enhanced by their Coulomb attraction [Eq. (2)], or coagulation between a 1-nm neutral particle and a negatively charged particle, enhanced by the image potential in the neutral particle [20]. The particles are assumed to have the same properties as bulk silicon.

negatively charged particle, Fig. 1 accounts for the image potential induced in the neutral, using the theory of Huang *et al.* [20]. (Note that for coagulation between oppositely charged particles there may be an image potential effect in addition to the ordinary Coulomb attraction. Moreover, screening of the plasma in the vicinity of either a charged particle or a neutral particle with an image potential may affect the enhancement in coagulation coefficients. To our knowledge, no analysis of coagulation in the literature includes these effects, and they are not included in the figure.)

As can be seen in Fig. 1, the coagulation coefficient for collisions between very small neutral particles and much larger charged particles is strongly enhanced by two effects that multiply together, the size dissimilarity and the image potential. For example, for the case of 1-nm-diameter neutral particles coagulating with 20-nm-diameter particles the former effect gives a factor of ~80 enhancement even for neutral-neutral coagulation, while the latter effect provides an additional enhancement factor of ~200. In fact, one sees that the enhancement in coagulation coefficients produced by the image potential is comparable in magnitude to that associated with the Coulomb attraction where one of the oppositely charged particles is singly charged. With this enhancement in coagulation coefficients, coagulation may occur fast enough to compete with diffusion as a sink for neutral particles.

In summary, this analysis indicates that coagulation in a nanodusty plasma may be possible provided that very small particles continue to be generated as larger, charged, and trapped particles continue to grow. Considering that neutral particles under conditions of interest are expected to be much more abundant than positively charged particles, and that Fig. 1 shows that the image potential in small neutrals can

have as much effect on coagulation as the Coulomb attraction associated with a single positive charge, a reasonable hypothesis is that coagulation is dominated by collisions between small neutral particles and large negatively charged particles.

III. NUMERICAL MODEL

In the present work we use the same numerical model as in Warthesen and Girshick [11], but with two important modifications. First, instead of limiting nucleation to a brief burst, it is allowed to continue in regions that are sufficiently free of particles. Second, we account for the effect on coagulation of the image potential induced in neutral particles in proximity to charged particles.

A detailed description of the numerical model is given in Warthesen and Girshick [11]. The geometry and conditions of the model are chosen to correspond to the experimental system of Boufendi, Bouchoule, *et al.* [1–3]: a parallel-plate capacitively coupled rf plasma, with rf power applied to one of the electrodes at a frequency of 13.56 MHz, and a voltage of 300 V (600 V peak to peak). The other electrode is grounded. The electrode spacing is 3 cm, the pressure equals 13.3 Pa, and the heavy species gas temperature equals 300 K.

As the parallel plates are assumed to be infinite the system is one dimensional. The plasma is assumed to consist of pure argon, in which silicon nanoparticles nucleate and grow. While the model can readily accommodate gas flow through one of the electrodes, the flow for these simulations is set to zero. The nanoparticles are transported by diffusion, electrostatic and ion drag forces. The effect of gravity is negligible for the particle sizes and conditions considered. The absence of gas flow thus creates a system that is symmetrical (for nanoparticles, which are too massive to respond to the instantaneous rf field) with respect to the midplane between the two electrodes.

This model does not include chemistry other than finite-rate ionization of argon atoms to generate positive ions and free electrons. In place of a detailed nucleation mechanism, silicon nanoparticles of diameter 0.75 nm are assumed to be formed by gas-phase nucleation at a prescribed rate. Nucleation is assumed to be confined to the central half of the electrode gap, roughly corresponding to the area between the plasma sheaths. Particles are allowed to grow by both coagulation and surface growth, with the latter also assumed to occur at a prescribed rate. For the simulation reported below, the nucleation rate is set to 10^{12} cm^{-3} s^{-1} and the surface growth rate is set to 12 nm s^{-1}. With these values the simulations reproduce approximately the measured particle concentrations and growth rates found in the studies of Bouchoule, Boufendi, *et al.* [1–3].

The nanoparticles are charged by collisions with ions and electrons, with orbital-motion-limited theory [21] used to predict the finite-rate charging behavior. The maximum charge possible on the particles depends on their size. Here we have used an expression specific to silicon particles developed by Gallagher [8], in which the charge is limited by the mutual electrostatic repulsion of the electrons and depends on the particle-size-dependent electron affinity.

The plasma and nanoparticle equations are solved in a two-step process. The electron balance and energy equations and the Poisson equation for the electric field are solved and averaged over several rf cycles. The resulting plasma properties are then used in solving the aerosol general dynamic equation for nanoparticle size and charge distributions in the reactor. A sectional model is used for discretizing the nanoparticle size distribution [22]. The Scharfetter-Gummel method is used to discretize the ion-, electron-, and nanoparticle-balance and electron-energy equations [23].

Two main changes have been made to the original model of Warthesen and Girshick [11]. First, the effect of the image potential on coagulation between neutral and charged particles, using the theory of Huang *et al.* [20], is now included. Second, whereas in Warthesen and Girshick [11] nucleation is confined to a burst lasting 10 ms, in the present simulations a more realistic condition is implemented such that nucleation is allowed to continue in regions that are relatively free of particles. In general, wherever condensible vapor or chemical species favorable to nucleation exist, there is a competition between homogeneous nucleation and heterogeneous surface growth on existing particles. Nucleation is quenched when the local particle surface area concentration is sufficiently high, as surface growth consumes these species [24]. To represent this, we have implemented a criterion such that, within the central half of the electrode gap, nucleation is turned on when (and only when) the local particle surface area concentration lies below a specified value S^*. Surface growth is turned on when (and only when) the local particle surface area concentration exceeds S^*. In the simulation discussed below the value of S^* is set to 1.8×10^9 nm^2 cm^{-3}, based on previous results of a detailed chemical kinetic model for nucleation and particle growth in a silane plasma for similar conditions [25]. Because particle trapping regions are predicted to be sharply defined, the simulation results are rather insensitive to the choice of this value.

These simulations are computation intensive. The simulation discussed below required approximately 1000 cpu hours on an SGI Altix per second of plasma time. Previous studies have developed numerical models for the chemical kinetics of particle nucleation and growth in a silane plasma that were either zero dimensional [25,26] or steady state [27,28]. At the present time, the inclusion of such detailed chemistry in one-dimensional, transient calculations such as presented here is not computationally feasible.

IV. RESULTS AND DISCUSSION

Figure 2 shows the simulation results for the particle size distribution function at four different times t following the onset of nucleation. White lines represent isocontours of average (negative) particle charge.

At $t=25$ ms most particles are smaller than 2 nm in diameter and contain zero or one charge. Stochastic charging is driven by high rates both of attachment and of neutralization. When particles become negatively charged they are pushed to the center by the electric field. Neutral particles diffuse

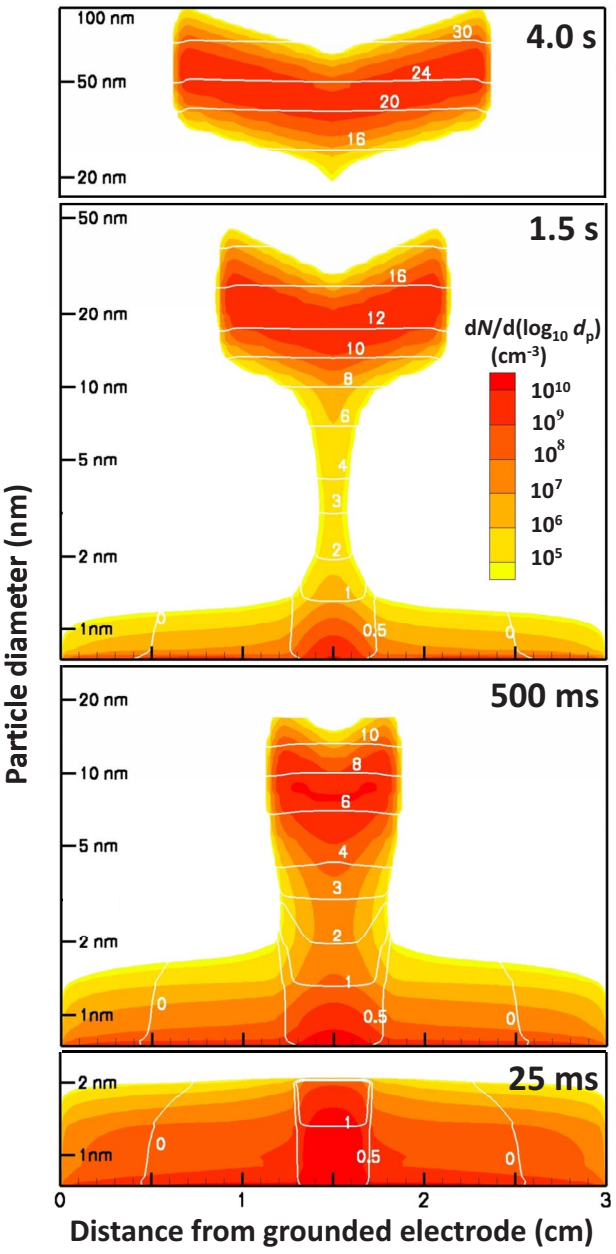

FIG. 2. (Color online) Nanoparticle size distribution function $[dN/d(\log_{10} d_p)]$ at 25 ms, 500 ms, 1.5 s, and 4.0 s following the onset of nucleation. White lines represent isocontours of average (negative) particle charge.

and positively charged particles are accelerated to the bounding electrodes.

As the particles grow and accumulate more negative charge, a bimodal particle size distribution develops at the center of the electrode gap, as seen in the snapshot at $t=500$ ms, where one peak in the distribution lies at a diameter of ~10 nm while a second peak exists at sub-nm size. The larger particles are those that have grown and become multiply negatively charged, and that are thus trapped in the center. Outside the central region, where the particle surface area concentration is small enough to allow fresh nucleation, those freshly nucleated particles that attach an electron are pushed to the center, forming the peak at sub-nm size.

At $t=1.5$ s the effect of ion drag has become evident. Ion drag pushes negatively charged particles out of the center and toward the plasma sheaths. The effect is stronger for larger, more highly charged particles, resulting in the "V" shape seen in the spatial profile of the size distribution function. As the particles spread outwards the region where nucleation is quenched expands, resulting in a reduction in the number of very small particles. Finally the entire plasma, up to the sheath edges, is filled with nanoparticles, which completely quenches nucleation at about 2.5 s. Past this time the small-size particle mode disappears, as evident in the snapshot at $t=4$ s, and particles are all negatively charged, and thus can grow only by surface growth.

Several aspects of the spatiotemporal evolution are similar to the earlier simulations of Warthesen and Girshick [11]. In particular, at the earliest times negatively charged particles are trapped in the center of the plasma, while at later times, when they have grown larger and become more charged, ion drag causes them to move toward the sheath edges, where the outward-pushing ion drag force is balanced by the inward-pushing electrostatic force exerted by the field at the sheath edge.

Other aspects of the predicted evolution are different in the current simulation compared to Warthesen and Girshick [11]. In particular, in the snapshots at 500 ms and 1.5 s, the bimodal size distributions seen in the center of the plasma, and the diffusion-dominated concentration profiles of very small neutral nanoparticles, are a consequence of the continued occurrence of nucleation outside the central trapping region.

However, as discussed below, the most important difference between the present results and those of Warthesen and Girshick [11] is that the earlier work predicted coagulation to be negligible, whereas the present simulation predicts an important role for coagulation.

Predicted concentration profiles of neutral, negatively charged and positively charged nanoparticles are shown in Fig. 3 at (a) 25 ms and (b) 1.5 s. At 25 ms the trapping of negative particles in the center of the electrode gap is evident, as is their outward spread at 1.5 s. The local peak in the center of the negatively charged particle concentration profile at 1.5 s is attributable to the small-particle mode in the particle size distribution at that time.

For neutral particles, the concentration profile at 25 ms is characteristic of a diffusion process, except for the small bump in the profile seen at the center. This bump is caused by neutralization of negatively charged particles, whose concentration is a maximum at the center. In contrast, at 1.5 s the maxima in the neutral particle concentration occur just outside the region where negatively charged particles are trapped. These maxima correspond to the locations where fresh nucleation occurs. These freshly nucleated particles diffuse both outward and inward. In addition, neutral particles can be created at the center by neutralization of singly charged negative particles.

Positively charged nanoparticles are predicted to exist at four to five orders of magnitude lower concentration than neutral particles. The shapes of the positive-particle concentration profiles at both 25 ms and 1.5 s are closely related to the corresponding ion density profiles, shown in Fig. 4. As

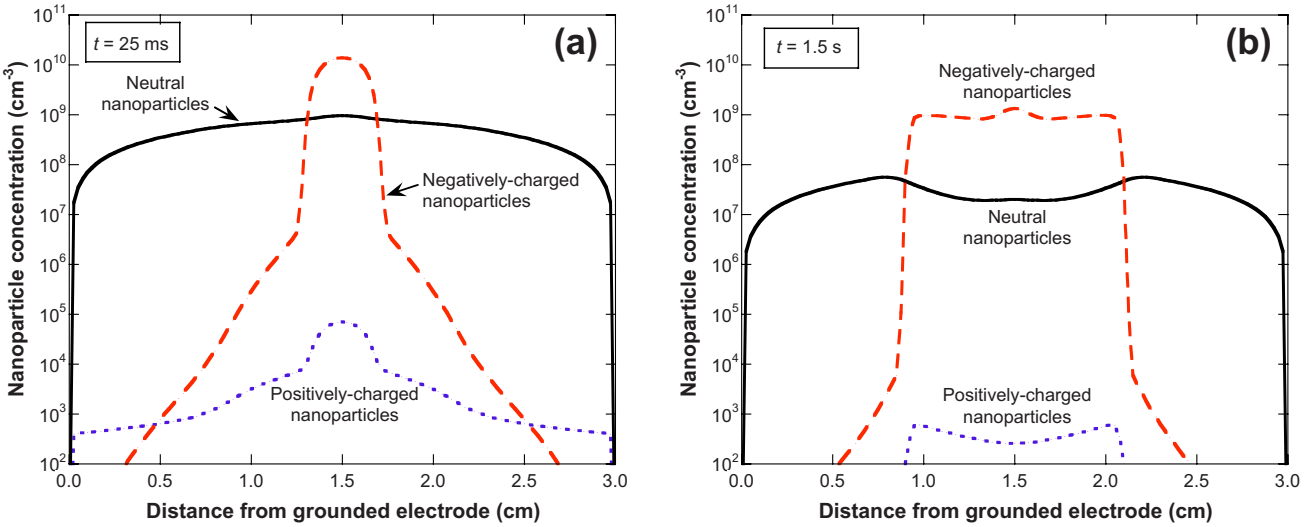

FIG. 3. (Color online) Concentration profiles of negatively charged, positively charged, and neutral nanoparticles at (a) $t=25$ ms and (b) 1.5 s following the onset of nucleation.

nanoparticles form and collect electrons, the electron density drops. In regions where negatively charged nanoparticles are trapped, they carry most of the negative charge, with the electron density lying about one order of magnitude below the charge density on the nanoparticles. As nanoparticles grow their spatial distribution changes. The ion density profile responds by closely tracking the changing profile of nanoparticle charge density, thereby maintaining quasineutrality. Peaks in the ion density profile correspond to regions of high ion attachment rates. Thus at 25 ms the peak in the center of the positively charged nanoparticle concentration profile corresponds to the peak in the ion density profile, while at 1.5 s the positively charged nanoparticle concentration profile mirrors the "V" shape in the ion density profile at that time.

The continual production of neutral nanoparticles by fresh nucleation allows for the possibility of coagulation. Figure 5 shows calculated spatial profiles of the coagulation rate at (a) 25 ms and (b) 1.5 s, together with corresponding concentration profiles of neutral and negatively charged nanoparticles. Consistent with the hypothesis that virtually all coagulation in this system occurs between neutral and negatively charged nanoparticles, coagulation is seen to be effectively confined to the region where negatively charged particles are trapped. At 25 ms the coagulation rate peaks sharply in the center of the plasma, a consequence of the multiplicative effect of the peaks in both the negatively charged and neutral particle concentration profiles. At 1.5 s the sharp off-center peaks in the coagulation rate profile are related to the coagulation coefficients shown in Fig. 1, as well as to the peak in the neutral particle concentration profile just outside the negative-particle trapping zone. As seen in Fig. 2, larger, more highly charged particles are pushed by ion drag farther from the center of the plasma than are smaller, less charged particles. The coagulation coefficient for coagulation of a 1-nm neutral particle with a charged particle is a strong func-

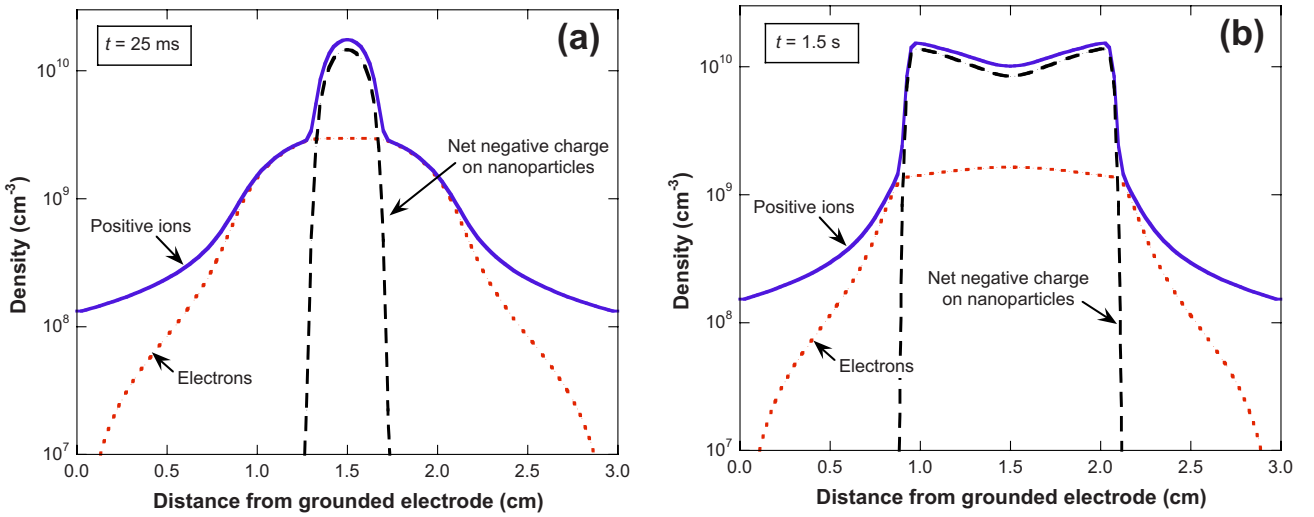

FIG. 4. (Color online) Profiles of charge densities carried by ions, electrons, and nanoparticles at (a) $t=25$ ms and (b) 1.5 s following the onset of nucleation.

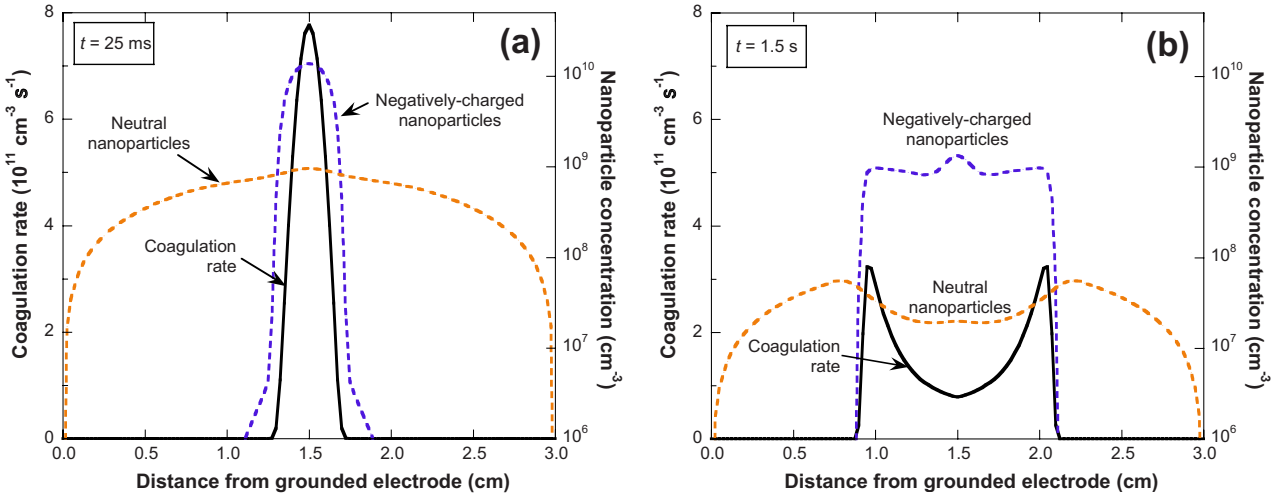

FIG. 5. (Color online) Profiles of particle coagulation rate at (a) $t=25$ ms and (b) 1.5 s following the onset of nucleation. Also shown are the concentration profiles of negatively charged and neutral nanoparticles.

tion of particle size and charge, especially in the diameter range below ~25 nm where most of the negatively charged particles lie at 1.5 s. This also explains why the coagulation rate at 1.5 s exhibits a minimum at the center of the plasma, even though the concentration of negatively charged particles has its maximum at that location: this maximum is due to the ~1-nm-diameter particle mode in the size distribution. From Fig. 1, the coagulation coefficient for a 1-nm neutral particle coagulating with a 1-nm charged particle is about two orders of magnitude lower than with a 20-nm-diameter charged particle, assuming that the charged particles contain the same charge as the average values in these simulations.

As the vast majority of coagulation events involve a neutral nanoparticle as one of the collision partners, it is of interest to ask how the coagulation rates calculated compare to the rates of loss of neutral nanoparticles to the electrodes by diffusion. Figure 6 shows this comparison versus time, over the 2.5 s before nucleation is completely quenched by the outward-spreading particle cloud. The rates shown in the figure are integrated over the electrode gap. At early times the diffusional loss rate is seen to be much greater than the coagulation rate. Gradually the coagulation rate increases and the diffusional loss rate drops. These rates become equal at ~400 ms. Thereafter the coagulation rate somewhat exceeds the diffusional loss rate, though both are of the same order. (Note that diffusional loss rates here are somewhat understated by the one-dimensional approximation, which implicitly neglects radial diffusion.) At ~2.5 s, when nucleation is completely quenched, both coagulation and diffusional loss go to zero, as both require the existence of neutral nanoparticles.

The reason for the rise in coagulation rates, and corresponding drop of diffusional loss rates, can be understood from Fig. 1: as trapped negatively charged particles grow, the coagulation coefficients for collisions between them and very small neutral nanoparticles strongly increase. It is thus evident that coagulation would be insignificant in this system were it not for the enhancement in coagulation coefficients caused by the image potential in small neutral nanoparticles.

Nor would coagulation be possible if nucleation were not sustained as the particle cloud develops. For the particular set of conditions and assumptions of this simulation, the average particle diameter at the time nucleation is quenched equals ~32 nm. Beyond this time, further coagulation would be essentially impossible unless nucleation resumed.

Indeed there is experimental evidence that nucleation in such systems could resume. At longer times one expects ion drag to push all nanoparticles out of the center, creating a void space. Experiments by Mikikian and Boufendi [29] have indicated that a new generation of nanoparticles can nucleate in such void spaces, and that the plasma can undergo multiple cycles of particle nucleation, growth, quenching of nucleation, appearance of a void space, and resumption of nucleation. The nature of coagulation in such a cyclic process will be the subject of future study.

V. SUMMARY AND CONCLUSIONS

A detailed numerical model has been used to investigate coagulation in a parallel-plate rf plasma undergoing particle

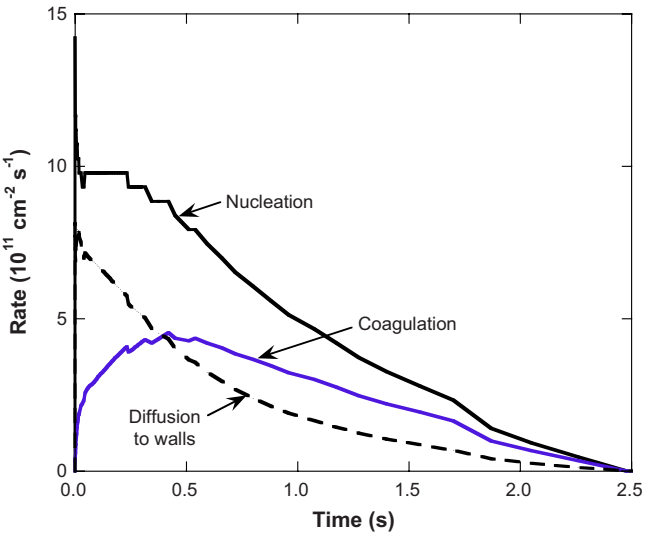

FIG. 6. (Color online) Rates of particle nucleation, loss of particles by diffusion to electrodes, and coagulation, integrated over electrode gap.

nucleation and growth. Simulation results indicate that coagulation is an important particle growth mode provided that two conditions exist: (i) that nucleation does not cease after a rapid burst but rather continues in the relatively particle-free regions outside particle trapping regions; and (ii) that coagulation coefficients between neutral and charged particles are enhanced by the image potential induced in the neutral particle. Under these conditions, we find that coagulation can "capture" many neutral nanoparticles before they are lost by diffusion, by joining them with a negatively charged, trapped nanoparticle. The simulations indicate that the coagulation rate exhibits a distinct spatial profile that reflects the sharply defined trapping regions of negatively charged nanoparticles as well as the profile of neutral nanoparticles. Coagulation is predicted to cease shortly following the quenching of nucleation by the expanding nanoparticle cloud, because the quenching of nucleation removes the source of neutral nanoparticles from the system.

These results appear to resolve the dilemma posed in the Introduction; how can significant coagulation occur in a nanodusty plasma? While no experimental study is yet available to test the validity of the spatiotemporal evolution in detail—it being difficult to obtain spatially resolved measurements of concentrations and size distributions of sub-10-nm aerosols in low-pressure environments—it can at least be noted that key aspects of the results are consistent with experimental or analytical results. The result that coagulation is significant for the first several seconds following the onset of nucleation, when particles have grown to several tens of nm in diameter, and then ceases, is in accord with experimental observations [1–7]. The effect of image potentials on coagulation assumed here is based on the best currently available theory [20]. The assumption that nucleation does not cease quickly after the onset of nucleation, but rather persists until being quenched by the particle cloud expanding to fill the plasma, is consistent with a large body of experimental observations for nucleating systems in general, and with previous theoretical analysis [24]. The existence in these types of plasmas of two distinctly different size classes, one small the other large, is supported by experimental observations [5,10].

A final interesting point is that these results explain why nanoparticles formed in low-pressure nonthermal plasmas are so often observed to be close to monodisperse, even though they show evidence of having undergone coagulation. "Normal" coagulation broadens a size distribution. However, the results presented here indicate that coagulation in nanodusty plasmas is dominated by very small neutral particles coagulating with larger, charged and trapped particles. Under such a situation, all trapped particles would grow at the same rate, as in particle surface growth, as long as they were in the same environment, consistent with the maintenance of a monodisperse size distribution.

ACKNOWLEDGMENTS

This work was partially supported by NSF Grant No. CBET-0756315 and by the University of Minnesota Supercomputing Institute (MSI). One of the authors, L.R., thanks Sarah Warthesen for helpful discussions and support with the numerical model and Shuxia Zhang at MSI for her help in using MSI computers for the simulations.

[1] A. Bouchoule and L. Boufendi, Plasma Sources Sci. Technol. **2**, 204 (1993).
[2] L. Boufendi and A. Bouchoule, Plasma Sources Sci. Technol. **3**, 262 (1994).
[3] L. Boufendi, J. Hermann, A. Bouchoule, B. Dubreuil, E. Stoffels, W. W. Stoffels, and M. L. d. Giorgi, J. Appl. Phys. **76**, 148 (1994).
[4] M. Shiratani, H. Kawasaki, T. Fukuzawa, H. Tsuruoka, T. Yoshioka, and Y. Watanabe, Appl. Phys. Lett. **65**, 1900 (1994).
[5] Y. Watanabe, M. Shiratani, H. Kawasaki, S. Singh, T. Fukuzawa, Y. Ueda, and H. Ohkura, J. Vac. Sci. Technol. A **14**, 540 (1996).
[6] C. Courteille, C. Hollenstein, J.-L. Dorier, P. Gay, W. Schwarzenbach, A. A. Howling, E. Bertran, G. Viera, R. Martins, and A. Macarico, J. Appl. Phys. **80**, 2069 (1996).
[7] H. Kawasaki, J. Kida, K. Sakamoto, T. Fukuzawa, M. Shiratani, and Y. Watanabe, J. Appl. Phys. **83**, 5665 (1998).
[8] A. Gallagher, Phys. Rev. E **62**, 2690 (2000).
[9] S. K. Friedlander, *Smoke, Dust and Haze: Fundamentals of Aerosol Dynamics* (Oxford University Press, New York, 2000).
[10] M. Shiratani, H. Kawasaki, T. Fukuzawa, T. Yoshioka, Y. Ueda, S. Singh, and Y. Watanabe, J. Appl. Phys. **79**, 104 (1996).
[11] S. J. Warthesen and S. L. Girshick, Plasma Chem. Plasma Process. **27**, 292 (2007).
[12] M. Horanyi and C. K. Goertz, Astrophys. J. **361**, 155 (1990).
[13] D. S. Lemons, R. K. Keinigs, D. Winske, and M. E. Jones, Appl. Phys. Lett. **68**, 613 (1996).
[14] L. Boufendi, A. Plain, J. P. Blondeau, A. Bouchoule, C. Laure, and M. Toogood, Appl. Phys. Lett. **60**, 169 (1992).
[15] K.-S. Kim and D.-J. Kim, J. Appl. Phys. **87**, 2691 (2000).
[16] D.-J. Kim and K.-S. Kim, AIChE J. **48**, 2499 (2002).
[17] K.-S. Kim, D.-J. Kim, J.-H. Yoon, J. Y. Park, Y. Watanabe, and M. Shiratani, J. Colloid Interface Sci. **257**, 195 (2003).
[18] K. De Bleecker, A. Bogaerts, and W. Goedheer, New J. Phys. **8**, 178 (2006).
[19] G. Lapenta, Phys. Scr. **57**, 476 (1998).
[20] D. D. Huang, J. H. Seinfeld, and K. Okuyama, J. Colloid Interface Sci. **141**, 191 (1991).
[21] J. E. Allen, Phys. Scr. **45**, 497 (1992).
[22] F. Gelbard, Y. Tambour, and J. H. Seinfeld, J. Colloid Interface Sci. **76**, 541 (1980).
[23] D. L. Scharfetter and H. K. Gummel, IEEE Trans. Electron Devices **16**, 64 (1969).
[24] M. K. Alam and R. C. Flagan, J. Colloid Interface Sci. **97**, 232 (1984).
[25] U. Bhandarkar, M. T. Swihart, S. L. Girshick, and U. Kortshagen, J. Phys. D **33**, 2731 (2000).

[26] U. Bhandarkar, U. Kortshagen, and S. L. Girshick, J. Phys. D **36**, 1399 (2003).
[27] K. de Bleecker, A. Bogaerts, and W. Goedheer, Phys. Rev. E **70**, 056407 (2004).
[28] K. De Bleecker, A. Bogaerts, R. Gijbels, and W. Goedheer, Phys. Rev. E **69**, 056409 (2004).
[29] M. Mikikian and L. Boufendi, Phys. Plasmas **11**, 3733 (2004).